Suppression of metal streak artifacts in CT using a MAP reconstruction procedure

Catherine Lemmens, David Faul, James Hamill, Sigrid Stroobants and Johan Nuyts

***Abstract*— Metal implants such as hip prostheses and dental fillings produce streak artifacts in the reconstructed CT images. Due to these streaks, the CT image may not be diagnostically usable. Therefore we propose a reconstruction procedure that diminishes the streak artifacts and that may improve the diagnostic value of the CT. The procedure starts with a MAP reconstruction using an iterative reconstruction algorithm and a multi-modal prior. This produces a streak-free starting image. This starting image will be the basis for a projection completion MAR procedure. The patient results are very promising but further investigation and validation is needed.**

I. Introduction

Filtered back projection (FBP) image reconstruction gives rise to streak artifacts in the presence of metal. Using a maximum-likelihood algorithm for monochromatic transmission tomography (MLTR) [1], [2] gives improved images but artifacts remain. Further improvement can be achieved by using a maximum likelihood algorithm that models the polychromatic nature of the CT radiation (IMPACT) [3]. However, even in simulations, some artifacts persist when IMPACT is started from a homogenous image. In contrast, when IMPACT is started from the correct solution, it converges to an only slightly different image. Moreover, if IMPACT is instructed to ignore the projections through the metal, it produces no changes when started from the correct solution.

These observations indicate that in the presence of metal objects, the CT data are incomplete, multiple solutions exist, and iterative reconstruction algorithms converge to a local maximum. In addition, it seems that the projections through the metal provide invalid information, and that it may actually be better to ignore them.

These findings suggest that an artifact-free reconstruction can be obtained, when a good starting image can be provided and the projections through the metal are ignored. However, when the reconstruction is not started from the correct solution, ignoring projections results in severe artifacts (black spots) around the ignored data region in the reconstruction. In the clinical data, the artifacts caused a great loss of detail in the surroundings of the metal and, moreover, such reconstructions wouldn't be usable for PET attenuation in PET/CT. Thus, in the clinical context, using the metal projections gives rise to streak artifacts, not using them gives rise to black spot artifacts. One solution to this problem has been projection completion [4], [5], [6], [7].

Considering all these findings, our approach to reduce the metal artifacts and to restore some of the diagnostic information, is creating a good, artifact-free starting image. This starting image will be used for two purposes. First, the projection completion will be based on this starting image rather than on sinogram-based interpolation. We expect that an image based method will give rise to an artificial sinogram that is more consistent than with a sinogram based approach. Second, based on the observations that a good input image can lead the MLTR algorithm to the exact solution, the starting image will be given as an input image for the final iterative reconstruction in an attempt to drive the algorithm towards a less artifact-prone solution.

The next section describes in more detail our metal artifact reduction (MAR) algorithm and especially the Maximum-A-Posteriori (MAP) [8] procedure to obtain the starting image.

II. Method

A. MAP procedure to obtain starting image

In the following, a description follows for obtainting a good starting image by incorporating some 'a-priori' knowledge in the iterative algorithm. In a patient, it is 'a-priori' known which pixel values to expect because the pixel values represent the attenuation values of the human tissues. So the most appropriate prior for inclusion of 'a-priori' knowledge seems to be an absolute intensity prior [9], [10]. This prior tends to assign each pixel value to one of the modes of the prior. The most obvious modes to choose are the attenuation coefficients μ of air, fatty tissue, soft tissue and bone (and some additional modes if their is lung tissue in the reconstructed image). The intensity priors are defined to behave as a Gaussian function with mean μ_i and standard deviation σ_i.

By using a multi-modal prior an artifact-free image can be produced. The disadvantage of such a prior is that fine details in the image may get lost when the prior is given a high weight. This is in contrast to our aim to recover as much detail as possible. However the absolute intensity prior is only used to produce the starting image, so the finer details can be recovered during the final reconstruction for which no prior is applied.

The reconstruction of the starting image consists of the following steps:

C. Lemmens, J. Nuyts and S. Stroobants are with the Dept. of Nuclear Medicine, K.U.Leuven, B-3000 Leuven, Belgium, (e-mail: catherine.lemmens@uz.kuleuven.be). D. Faul and J. Hamill are with Siemens Medical Solutions, MI, Knoxville, TN, USA. This work is supported by F. W. O. (Flemish research fund) grant G.0174.03, by Siemens Medical Solutions, and, by 2006 IEEE NSS-MIC Trainee Award.

1) Initial reconstruction with MLTR.
2) Thresholding of the initial reconstruction to divide the image in different classes so that a label-image is formed.
3) For each class, an absolute intensity prior is defined.
4) MAP reconstruction based on the defined multi-modal priors to obtain the starting image.

In the following each of these steps is described in more detail.

1) Initial reconstruction: The CT fan beam sinograms are rebinned to a parallel beam configuration. The initial image is then reconstructed with MLTR using 370 iterations accelerated with subsets [11]. The "raw" CT data obtained from the scanner have actually undergone several corrections, including the subtraction of a background from each detector reading, the crosstalk correction, off-focal radiation correction, beam hardening correction, the log-conversion, converting the measured intensities to the integrals of attenuation coefficients, azimuthal smoothing, and, in some scanners, ring removal. The MLTR algorithm starts from a blank and a transmission sinogram, assuming that the blank sinogram is noise-free, while the transmission sinogram values are samples from a Poisson distribution. Although the real distribution is not exactly Poisson, the approximation is reasonable, and rightly assigns a lower signal-to-noise ratio to values corresponding to higher attenuation. In order to apply MLTR to the CT-data, an arbitrary noise-free blank scan of 10^5 photons per detector pixels is introduced. The transmission scan is calculated as $y_i = b_i \exp(-r_i)$, where b_i is the blank scan value for detector element i, r_i is the "raw" CT-value and y_i the computed transmission value. In the case of metal artifacts and truncation, MLTR reconstructions will be superior to FBP (Filtered Back Projection). During FBP reconstruction all projections receive the same weight whereas with MLTR, the projections through metal are rightly assigned a lower weight [12], resulting in less artifacts. The top left image of fig. 1 shows an initial reconstruction.

2) Thresholding and defining the label image: The initial image is then thresholded for metal. The threshold currently used is 0.8 cm^{-1}, which is almost twice the linear attenuation value of bone. By setting all metal pixels to one and all other pixels to zero, a binary image of the metal is created. By forward projection of this metal image, the corresponding projections of the metal in the original sinogram data can be identified.

Based on the metal image, a three-label image is created. All pixels in the initial image are assigned one of the values 0, 1, or 2 based on their attenuation value and on their location with respect to the metal pixels. By thresholding the initial reconstruction all patient body pixels can be obtained and, when applicable, the patient bed can be identified. These pixels are assigned the value 2. Then the surrounding pixels of the metal, which thus originally have the value 2, are assigned the value 1. This area is created automatically by expanding the metal region by a pre-defined amount. In the case of a patient with multiple dental fillings on both sides of the jaw, this expansion is wide enough to encompass all the pixels lying in between the opposing dental fillings. Pixels outside the patients body are assigned the value 0, as well as the metal pixels themselves. The middle right panel of fig. 1 shows such a label image, (pixels with value 2 are white, pixels with value 1 are grey and pixels with value 0 are black).

3) Defining the multi-modal priors: For each label, a corresponding absolute intensity prior is defined. For label 2, containing most of the patient, a multi-modal prior is defined which has the modes air, fat tissue, soft tissue and bone. For label 1, the vicinity of the metal, only the modes soft tissue and bone are used. The reason air is not included as a mode, is because we do not want any black spots or streaks, which are common artifacts in the surroundings of the metal, in the starting image. For label 0, which contains the metals and the area around the patient, no prior is defined. We do not care which values the MLTR reconstruction assigns to the metal pixels because after the MAP reconstruction, metal pixels will be replaced by the values of a less dense object.

4) MAP reconstruction: Finally, the starting image is obtained by performing a MAP reconstruction based on the priors defined on the label-image. The MAP objective function has the following form:

$$\Phi(\mu) = L(y|\mu) + \beta \ln p(\mu)$$

where μ is the image distribution, y is the measured transmission data, $L(y|\mu)$ is the log-likelihood and $p(\mu)$ is the prior distribution with β the weight given to this prior information. The prior distribution $p(\mu)$ is defined as a combination of Gaussians with mean μ_i and standard deviation σ_i:

$$p(\mu) = \sum_{i=1}^{M} \frac{S_i(\mu)}{\sqrt{2\pi}\sigma_i} \exp \frac{(\mu - \mu_i)^2}{2\sigma_i^2}$$
$$\sum_{i=1}^{M} S_i(\mu) = 1$$
$$S_i(\mu) = 1 \quad \text{if} \quad \mu_i - t_i < \mu < \mu_{i+1} - t_{i+1},$$
$$\text{else} \quad S_i(\mu) = 0$$
$$\text{and} \quad t_1 = -\infty, \quad \mu_{M+1} = \infty, \quad t_{M+1} = 0$$

with t_i the intersection points of neighboring Gaussians, and S_i determine which Gaussians (or mode) is used. The standard deviation σ_i determines the weight that is given to each mode, so different modes can have different individual weights, but the global weight β of each mode is the same. The lower the standard deviation, the more a pixel will be attracted towards the mean value of that mode. The intersection points t_i are standardly chosen in the middle of two modes, so that each mode has the same range. However here, the range of the soft tissue mode is defined to be wider than that of the other modes.

For this MAP-reconstruction the initial image serves as an input image and the MAP-reconstruction is obtained with 100 iterations accelerated with subsets. By including this prior information, the MAP reconstruction is forced toward a reconstruction that is streak-free and has no black spots near the metal. The bottom left panel of fig. 1 shows such a starting image.

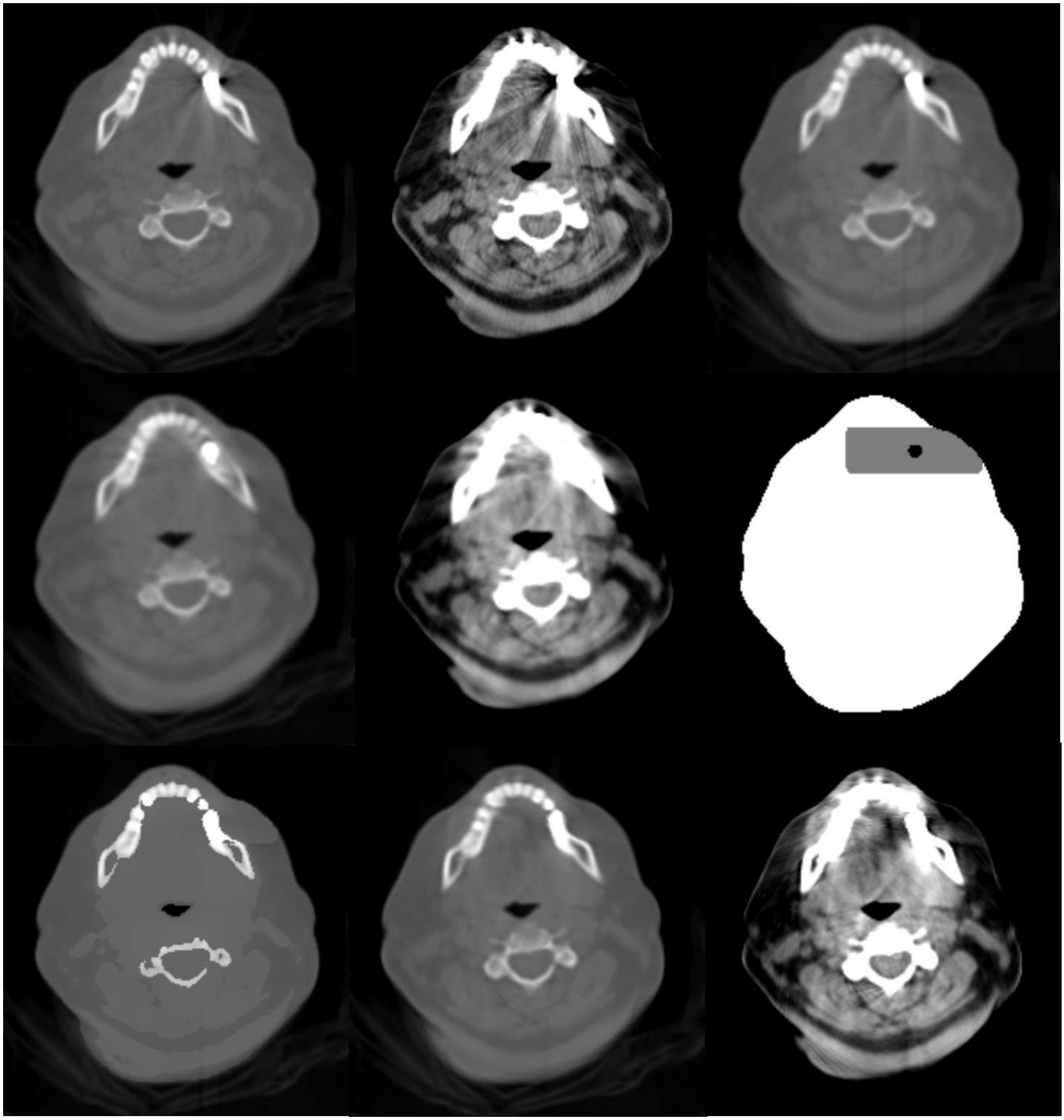

Fig. 1. Total MAP-reconstruction procedure: Top left and middle shows the FBP reconstruction with respectively bone and soft tissue window, top right shows the initial MLTR-reconstruction, middle row left and middle show the linear interpolation reconstruction with respectively bone and soft tissue window, middle right row shows the label-image, bottom left shows the starting image, bottom middle and right shows the final reconstruction with respectively bone and soft tissue windowTop left shows the FBP reconstruction, top right shows the initial MLTR-reconstruction, middle left shows the linear interpolation reconstruction, middle right shows the label image, bottom left shows the starting image, bottom right shows the final reconstruction

B. Projection completion

The metal pixels in the starting image are replaced by pixel values of 0.8 cm^{-1}. So the original metal is replaced by a less dense object with the same shape as the metal. By choosing this high value, it is still possible to identify the metal region after the final reconstruction. Then, this slightly modified starting image is forward projected to form the ”artificial” sinogram. In step 2 of the MAP procedure to form the starting image,

the metal projections were identified in the original sinogram. These metal projections in the original data are now replaced by the corresponding projections of the artificial sinogram. However, the transition between the original data and the replaced data should be continuous in order to avoid introducing artifacts. To ensure this smoothness, a linear interpolation is made between the original data and the artificial data in the data points neighboring the metal projections. A sinogram, where the corrupted metal projections are replaced by the projections of a dense object, is obtained.

C. Final reconstruction

The final reconstruction using the projection completed data is done with MLTR or IMPACT using 750 iterations accelerated with subsets. A smoothed version of the modified starting image is given as input image for this reconstruction. The bottom right image in fig. 1 shows the final result.

III. Results

The results on two clinical patient studies are presented. The patients were scanned with a Siemens Biograph 16 PET/CT system. The CT data were exported so that off-line reconstruction with our software was possible.

A. Patient with dental fillings

Fig. 2 shows the results obtained in a patient with multiple dental fillings. The top left and middle panel show the metal artifacts when reconstruction is performed with FBP. When reconstruction is performed with MLTR, shown in the top right panel of fig. 2, there is some small improvement. The result of our MAR algorithm is shown in the bottom middle and right panel of fig. 2. The black-white streaks are strongly reduced and details in between the metals are partially restored. Some fine streaks still persist but nevertheless the improvement is significant. The middle right panel of fig. 2 shows the label-image which was used and the bottom left panel shows the starting image obtained with the MAP reconstruction.

B. Patient with two hip prostheses

Fig. 3 shows the results obtained in a patient with two hip prostheses. The top panel shows the metal artifacts when reconstruction is performed with FBP. A broad, dark band is apparent in the region connecting the two hips. When reconstruction is performed with MLTR, shown in the second row left of fig. 3, there is some small improvement but the dark band is still visible. The result of our MAR algorithm is shown in the fourth row right and in the bottom right panel of fig. 3. The dark band is strongly reduced. However pixel values in between the hip are still somewhat lower than their surroundings.

C. Comparison with projection completion based on linear interpolation

By forward projection of the metal image (see step 2 of the MAP-procedure) a mask of the metal in the sinogram is produced. When the projection completion is performed based on linear interpolation, all sinogram values within that mask are replaced by linear interpolation between the nearest values outside the mask [6]. Finally, the mask multiplied with an arbitrary density D is added to the interpolated sinogram [12]. The reconstruction of this interpolated sinogram is done with MLTR.

The middle left panels of fig. 1, 2 and 3 show the results when projection completion is based on linear interpolation. In the case of dental fillings, our MAR approach shows better restoration of the teeth, more details in between the teeth with dental fillings and fewer streaks than the linear interpolation method. In the case of the hip prostheses, there are some significant differences between the two methods in the area of the right hip. However, because the ground truth is not known, it is hard to decide which one is actually better.

IV. Discussion

We present here a fully automated reconstruction procedure for MAR. There are no parameters that need to be adjusted manually during reconstruction. The time needed for the reconstruction of one slice is 1 to 2 minutes on a 3 GHz PC. IMPACT is three to four times slower than MLTR, so using IMPACT for the final reconstruction would further increase the reconstruction time. However, in this study, no significant differences between MLTR and IMPACT reconstruction were observed. This indicates that the beam hardening correction applied by the manufacturer removed all the beam hardening effects or, that beam hardening was not the major cause of the metal artifacts.

One could use FBP instead of MLTR for the initial reconstruction to speed up the algorithm. However, artifacts are more severe with FBP, so that the bright streaks artifacts could alias as metal after thresholding. Another option is to reduce the number of iterations in the initial reconstruction. This initial reconstruction is already a high quality image, but probably a lower quality image would result in the same starting image.

By using an absolute intensity prior, in each iteration the algorithm will tend to attribute one of the modes to each pixel. Therefore the use of such a prior could be seen as a segmentation of the image in different tissue classes. However the difference with a real segmentation is that there still exists some variation in the pixel values belonging to the same class, especially when the prior is given a low weight.

In the case of the hip prostheses, pixel values in between the two hips were somewhat lower than the values of their surrounding. This is partially due to the starting image. As seen in the bottom left panel of fig. 3 the MAP reconstruction has falsely assigned fat tissue values instead of soft tissue values to the pixels lying in the middle of the two hip prostheses.

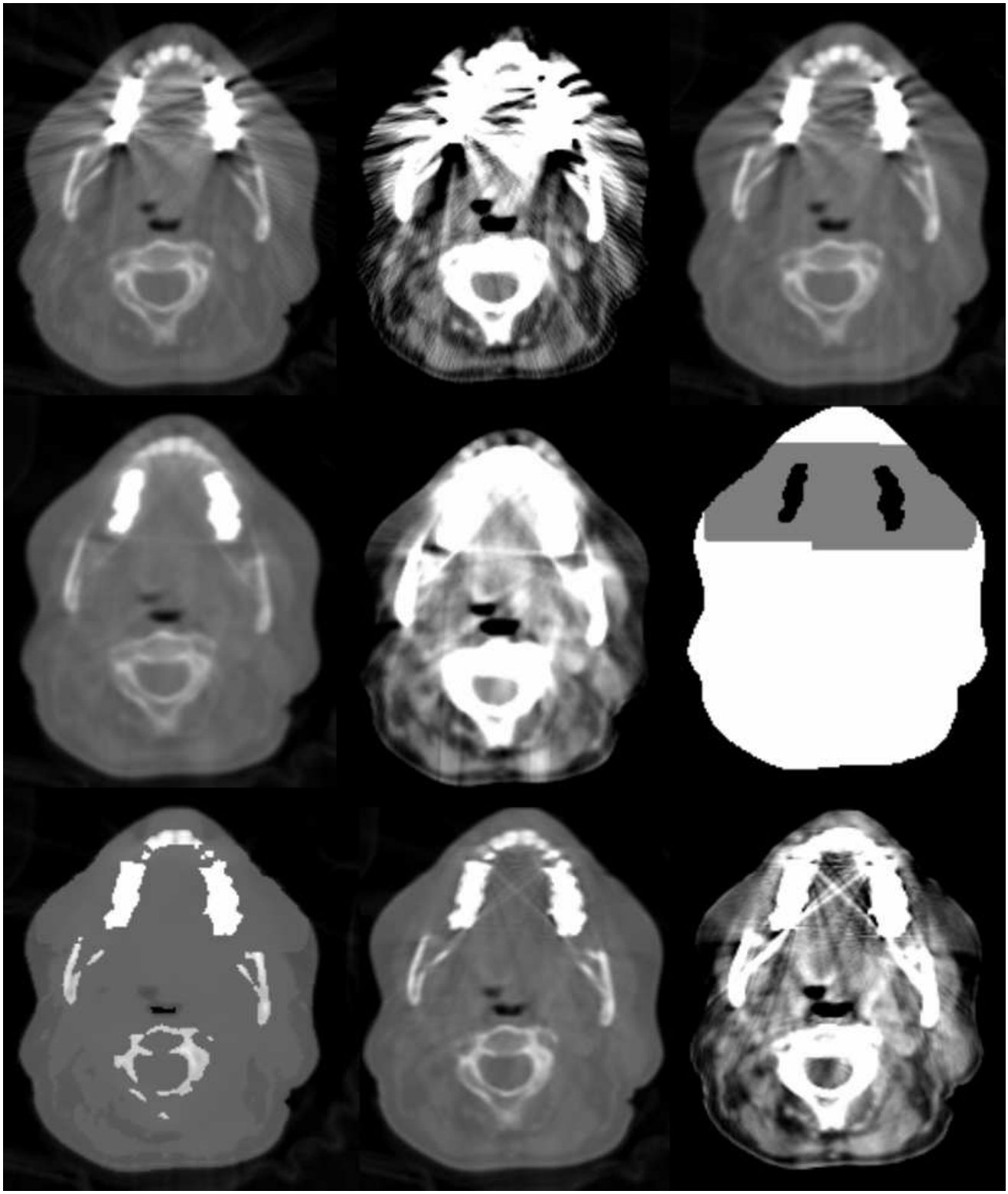

Fig. 2. Patient with dental fillings: Top left and middle shows the FBP reconstruction with respectively bone and soft tissue window, top right shows the initial MLTR-reconstruction, middle row left and middle show the linear interpolation reconstruction with respectively bone and soft tissue window, middle right row shows the label-image, bottom left shows the starting image, bottom middle and right shows the final reconstruction with respectively bone and soft tissue window

The use of projection completion is a popular way to suppress metal artifacts. One of the simplest methods is to use

linear interpolation between the nearest neighboring projections unaffected by the metal [6]. Here we compared our MAR algorithm with this method. Results show that our method gives improved results: less streaks, more details are recovered and in the case of dental fillings, the teeth are better restored. In the literature more complex interpolation schemes are presented [7], [13], [14], all giving improved results over linear interpolation.

A MAR algorithm similar to ours is developed by Bal and Spies [15]. They perform a segmentation of the image, replace the metal with soft tissue and do a forward projection of this modified image. Then they replace the metal projections by the corresponding projections of the segmented image. Reconstruction is done with FBP. However in the case of strongly distorted images their segmentation is not perfect and black spots remain. Our starting images don not suffer from this problem because we forbid the MLTR algorithm to create black spots or streaks near the metal by applying a prior with only the modes bone and soft tissue in the surroundings of the metal. However as seen in the case of the two hip prostheses our segmentation isn't perfect either as it attributes fat tissue values instead of soft tissue values in between the hips. In contrast to our MAR algorithm, they replace the metal pixels with soft tissue and use FBP for reconstruction. Because we replace the metal with a dense object and reconstruct with MLTR, the projection completed data are given a lower weight during the reconstruction and are thus considered to be less reliable, which should help to suppress the artifacts.

Reduction of the metal artifacts is not only important for the diagnostic value of the CT but also plays a major role in PET/CT. Due to the metal and the metal artifacts, the PET attenuation map derived from the CT image by applying the hybrid scaling method [16] is inaccurate. The PET attenuation values of metals are overestimated which results in increased Standard Uptake Values (SUVs). These increased SUVs can falsely be diagnosed as lesions. In order to exclude these false positive lesions, the PET image reconstructed without attenuation correction has to be consulted. On the other hand, the dark streaks in the CT image result in an underestimation of the PET attenuation values resulting in decreased SUVs.

If only a PET image is required without a diagnostic CT image, the diagnostic CT image is downsampled to PET resolution and then converted to PET attenuation values. However we think that it is feasible to perform the attenuation correction based on a downsampled version of our modified starting image. The use of an absolute intensity prior will probably also improve the attenuation map quality when a low mAs CT scan is performed.

V. Future work

We plan on validating our MAR algorithm by simulations and phantom studies. With the simulations we want to confirm the ability of the algorithm to restore diagnostic detail in the neighborhood of metals and in the regions in between two or more metals. With the phantom study, we hope to demonstrate that the algorithm can suppress the metal artifacts and that it is usable for attenuation correction in PET/CT.

Further, the performance of our algorithm will be compared with projection completion based on the interpolation scheme presented in [7] in a clinical study containing 40 patients.

In the cases where there is very little metal, like the case of one dental filling, and/or when the metal is not very dense, we think that the metal projections may still contain some usable information which will be lost when projection completion is performed. Therefore in the future, we will try to develop a MAP reconstruction procedure using all of the original data in order to suppress the metal artifacts.

VI. Conclusion

We have proposed a MAR algorithm that basically consists of two steps: One, the creation of a good starting image using a MAP reconstruction procedure, and two, performing projection completion based on the modified starting image. The results presented here show that our MAR algorithm performs well. Further investigation and validation are planned.

References

[1] B. De Man, J. Nuyts, P. Dupont et al., "Reduction of metal streak artifacts in x-ray computed tomography using a transmission maximum a posteriori algorithm", *IEEE Trans Nucl Sci*, vol. 47 (3), 977-981, 2000.

[2] J. Nuyts, B. De Man, P. Dupont, M. Defrise, P. Suetens and L. Mortelmans, "Iterative reconstruction for helical CT: a simulation study", *Phys Med Biol*, vol. 43, 729-737, 1998.

[3] B. De Man, J. Nuyts, P. Dupont et al., "An iterative maximum-likelihood polychromatic algorithm for CT", *IEEE Trans Med Imaging*, vol. 20 (10), 999-1008, 2001.

[4] R. M. Lewitt and R. H. Bates, "Image reconstruction from projections: III: Projection completion methods (theory)", *Optik*, vol. 50, 189-204, 1978.

[5] G. H. Glover and N. J. Pelc, "An algorithm for the reduction of metal clip artifacts in CT reconstructions", *Med Phys*, vol. 8 (6), 799-807, 1981.

[6] W. A. Kalender, R. Hebel and J. Ebersberger, "Reduction of CT artifacts caused by metallic implants", *Radiology*, vol. 164, 576-577, 1987.

[7] A. H. Mahnken, R. Raupach, J. E. Wildberger et al., "A new algorithm for metal artifact reduction in computed tomography: In vitro and in vivo evaluation after total hip replacement", *Invest Radiol*, vol. 38 (12), 769-775, 2003.

[8] J. Qi and R. M. Leahy, "Iterative reconstruction techniques in emission computed tomography", *Phys Med Biol*, vol. 51, R541-R578, 2006.

[9] Z. Liang, R. Jaszczak, R. Coleman and V. Johnson, "Simultaneous reconstruction, segmentation, and edge enhancement of relatively piecewiece continuous images with intensity-level information", *Med Phys*, vol. 18 (3), 394-401, 1991.

[10] J. Nuyts, P. Dupont, S. Stroobants et al., "Simultaneous maximum a posteriori reconstruction of attenuation and activity distributions from emission sinograms", *IEEE Trans Med Imaging*, vol. 18 (5), 393-403, 1999.

[11] H. M. Hudson and R. S. Larkin, " Accelerated image reconstruction using ordered subsets of projection data", *IEEE Trans Med Imaging*, vol. 13 (4), 601-609, 1994.

[12] J. Nuyts and S. Stroobants, "Reduction of attenuation correction artifacts in PET-CT", *IEEE NSS-MIC*, proceeding, 2005, 1895-1899.

[13] M. Yazdia, L. Gingras and L. Beaulieu, "An adaptive approach to metal artifact reduction in helical computed tomography for radiation therapy treatment planning: experimental and clinical studies", *Int J Radiat Oncol Biol Phys*, vol. 62 (4), 1224-1231, 2005.

[14] M. Oehler and T. M. Buzug, "Modified MLEM algorithm for artifact suppression in CT", *IEEE NSS-MIC*, abstract M16-1, 2006.

[15] M. Bal and L. Spies, "Metal artifact reduction in CT using tissue-class modeling and adaptive prefiltering", *Med Phys*, vol. 33 (8), 2852-2859, 2006.

[16] P. Kinahan, D. Townsend et al., "Attenuation correction for a combined 3D PET/CT scanner", *Med Phys*, vol. 25, 2046-2053, 1998.

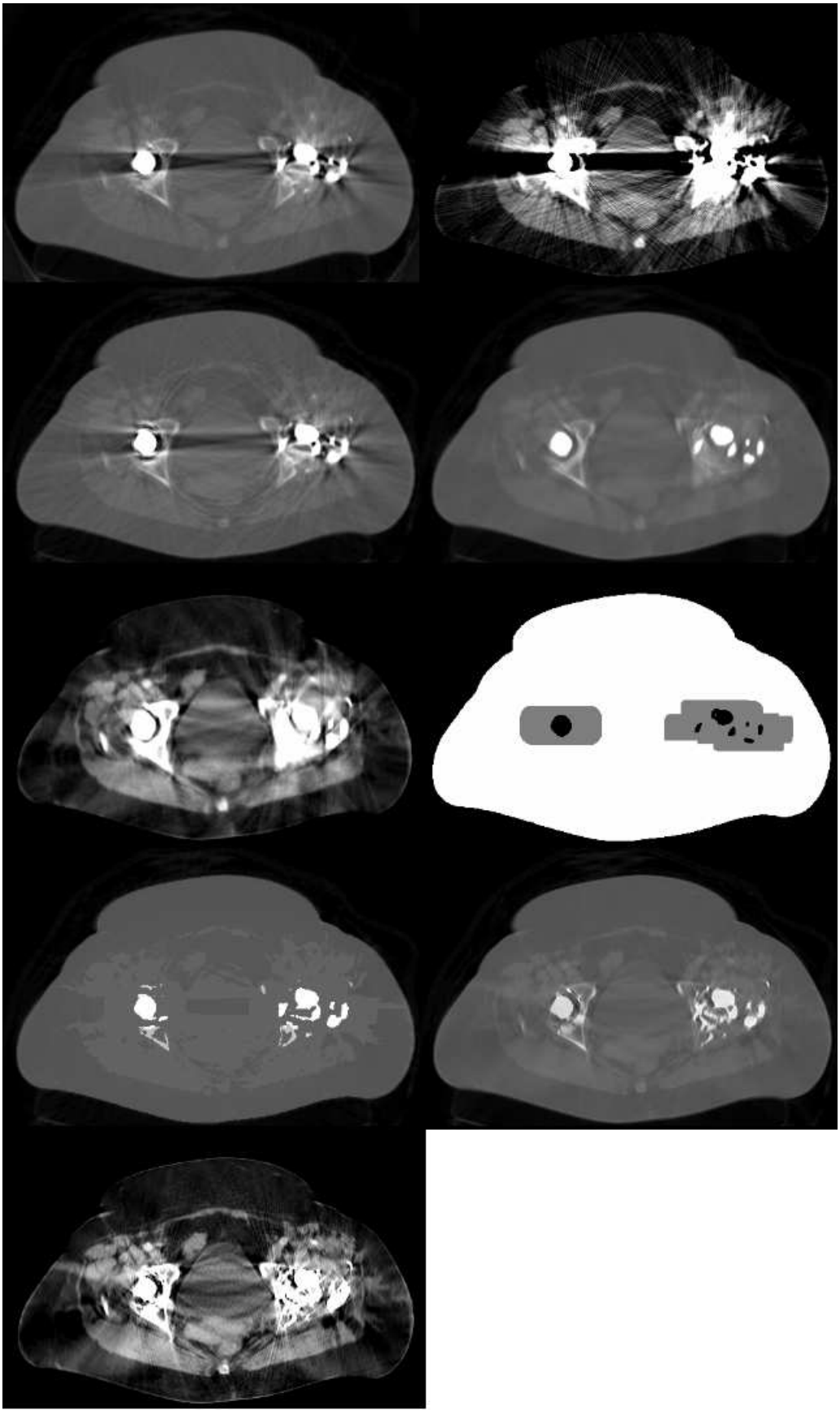

Fig. 3. Patient with two hip prostheses: Top left and right shows the FBP reconstruction respectively with bone and soft tissue window, second row left shows the initial MLTR-reconstruction, second row right shows shows the linear interpolation reconstruction with bone window, third row left shows the linear interpolation reconstruction with soft tissue window, third row right shows the label-image, fourth row left shows the starting image, fourth row right shows the final reconstruction with bone window and bottom left shows the final reconstruction with soft tissue window.